INTERNATIONAL JOURNAL FOR NUMERICAL METHODS IN FLUIDS
Int. J. Numer. Meth. Fluids **26**: 751–769 (1998)

NUMERICAL ANALYSIS OF BREAKING WAVES USING THE MOVING PARTICLE SEMI-IMPLICIT METHOD

SEIICHI KOSHIZUKA*, ATSUSHI NOBE AND YOSHIAKI OKA

Nuclear Engineering Research Laboratory, The University of Tokyo, 2-22 Shirane, Shirakata, Tokai-mura, Naka-gun, Ibaraki-ken 319-11, Japan

SUMMARY

The numerical method used in this study is the moving particle semi-implicit (MPS) method, which is based on particles and their interactions. The particle number density is implicitly required to be constant to satisfy incompressibility. A semi-implicit algorithm is used for two-dimensional incompressible non-viscous flow analysis. The particles whose particle number densities are below a set point are considered as on the free surface. Grids are not necessary in any calculation steps. It is estimated that most of computation time is used in generation of the list of neighboring particles in a large problem. An algorithm to enhance the computation speed is proposed. The MPS method is applied to numerical simulation of breaking waves on slopes. Two types of breaking waves, plunging and spilling breakers, are observed in the calculation results. The breaker types are classified by using the minimum angular momentum at the wave front. The surf similarity parameter which separates the types agrees well with references. Breaking waves are also calculated with a passively moving float which is modelled by particles. Artificial friction due to the disturbed motion of particles causes errors in the flow velocity distribution which is shown in comparison with the theoretical solution of a cnoidal wave. © 1998 John Wiley & Sons, Ltd.

KEY WORDS: MPS; particle method; incompressible flow; free surface; breaking wave; surf similarity parameter

1. INTRODUCTION

The moving particle semi-implicit (MPS) method was developed for incompressible flow with free surfaces [1–3]. In the MPS method fluids are represented by particles. Governing equations are discretized by particle interaction models the authors have developed. Grids are not necessary. A semi-implicit algorithm is employed to simulate incompressibility. Basic problems were solved to verify the particle interaction models used in the MPS method [1–3]. The weight function which was used in the particle interaction models was improved to enhance the numerical stability of the MPS method [4]. Collapse of a water column was solved and compared with an experiment. The shape of free surfaces agreed well with the experimental result, even if fragmentation and coalescence of the fluid occurred.

In the MPS method the computation time is relatively short because all particle interaction models developed are macroscopic and deterministic. Nevertheless, the MPS method requires additional computation time for the generation of the neighbor list, in which the neighboring

* Correspondence to: Nuclear Engineering Research Laboratory, The University of Tokyo, 2-22 Shirane, Shirakata, Tokai-mura, Naka-gun, Ibaraki-ken 319-11, Japan. Tel.: +81 29 2878441; Fax: +81 29 2878488; E-mail: koshi @ tokai.t.u-tokyo.ac jp

CCC 0271–2091/98/070751–19$17.50

Received September 1996
Revised April 1997

particle numbers are recorded. Distances of all pairs of particles should be calculated to generate the list. Since this calculation requires the scale of N^2 operations in each time step, it is dominant for the computation time in large problems. In the present study, an algorithm is proposed to reduce the count of operations to the scale of $N^{1.5}$.

Free surface flows have been solved by numerical methods using grids. It has been difficult to calculate breaking waves because fluid fragmentation and coalescence occur on the free surface. Breaking waves were analyzed with stationary grids [5]. The free surface was represented by a polygon composed of segments, the motion of which was calculated in each time step. Overturning of a wave was successfully calculated, but subsequent coalescence of the fluid was not calculated. Calculation procedures of the cells involving the segments were complicated. A plunging breaker was calculated by the marker-and-cell (MAC) method [6]. The markers representing the existence of the fluid move according to the flow field, which is solved using the grid. The coalescence of the overturning fluid was calculated by markers. The MAC method was used with unstructured grids to calculate free surface flows in a curved tank [7]. In the MAC method, fluid fragmentation and coalescence on the free surfaces can be solved, although the cells involving markers still need complicated treatment. The volume-of-fluid (VOF) method was applied to free surface flows with fluid fragmentation [8]. Breaking waves were analyzed using the VOF method [9,10]. A scalar quantity representing the volume of fluid is introduced to a stationary grid. The free surface is not clear due to the numerical diffusion derived from the advection terms of the scalar quantity. The calculation procedure of the cells involving the free surface is also complicated. Interactions between non-linear waves and permeable submerged breakwaters were calculated, but wave breaking was not dealt with [11,12].

In the present paper, numerical simulation of breaking waves using the MPS method is presented. The relation between the breaker types and the surf similarity parameter is compared with the experiments in References [13,14]. The experiments were carried out using wave tanks. One side of the tank had a piston which generated waves. These waves travelled to the slope on the other side. Breaking waves with a passively moving float are also calculated to show the possibilities of the MPS method for fluid–structure interaction problems with free surfaces. Two-dimensional non-viscous incompressible flows are analyzed in this study.

2. NUMERICAL METHOD

2.1. Governing equations

Governing equations are expressed by conservation laws of mass and momentum. Incompressible non-viscous flows are considered in this study:

$$\frac{\partial \rho}{\partial t} = 0, \tag{1}$$

$$\frac{D\mathbf{u}}{Dt} = -\frac{1}{\rho}\nabla P + \mathbf{f}, \tag{2}$$

where, ρ denotes the density, P the pressure, $\mathbf{u}$ the velocity, and $\mathbf{f}$ the external force.

The mass conservation equation is represented by density, while velocity divergence is usually used in the finite difference method. The left side of Equation (2) is the Lagrangian time differentiation involving advection terms. In MPS the advection terms are directly incorporated into the calculation by moving particles. Only gravity is considered as the external force. Two-dimensional problems are solved in this study.

2.2. Particle interaction models

A particle interacts with its neighboring particles covered with a weight function $w(r)$, where r is a distance between two particles. The weight function employed in this study is as follows (Figure 1):

$$w(r) = \begin{cases} \dfrac{r_e}{r} - 1 & 0 \leq r < r_e \\ 0 & r_e \leq r \end{cases}. \tag{3}$$

Interactions are restricted to a finite distance r_e. Thus, a finite number of neighboring particles are related to the interactions. The operation count of interactions is the scale of NM, which saves the computation time in large problems. Here, N is the total number of particles and M is the average number of neighboring particles within a distance of r_e; actually the number of neighboring particles varies around M. If the weight function is not limited with respect to r, the operation count is the scale of N^2. Another important aspect of the weight function is that it is infinity at $r = 0$. This is good for avoiding clustering of particles, which is explained later.

When a particle i and its neighbors j are located at $\mathbf{r}_i$ and $\mathbf{r}_j$, particle number density is defined as,

$$\langle n \rangle_i = \sum_{j \neq i} w(|\mathbf{r}_j - \mathbf{r}_i|) \tag{4}$$

The number of particles in a unit volume, ρ_n, can be approximated by the particle number density:

$$\langle \rho_n \rangle_i = \frac{\langle n \rangle_i}{\int w(r)\, \mathrm{d}v}. \tag{5}$$

The denominator of the right side of Equation (5) is the integration of the weight function over the whole area. This integration is constant if r_e is fixed. Then the fluid density, ρ, is expressed as,

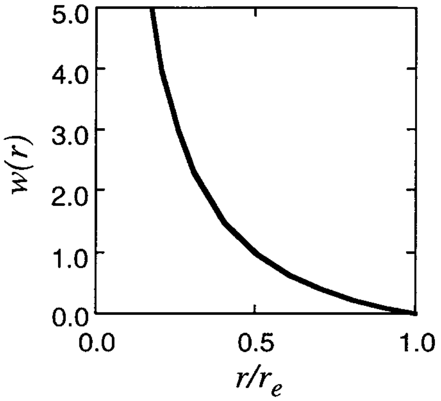

Figure 1. Weight function.

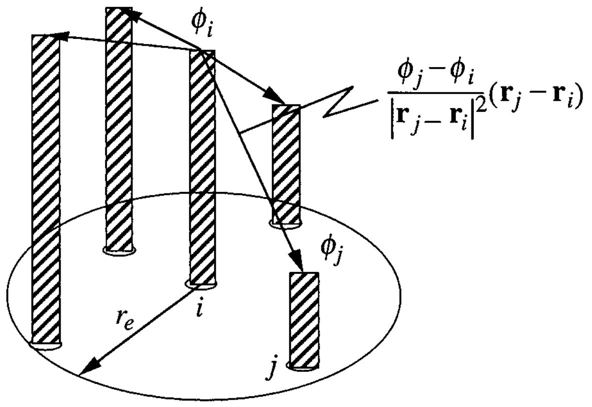
ϕ_i
$\frac{\phi_j-\phi_i}{|\mathbf{r}_j-\mathbf{r}_i|^2}(\mathbf{r}_j-\mathbf{r}_i)$
ϕ_j
r_e
i
j

Figure 2. Concept of gradient model.

$$\langle\rho\rangle_i = m\langle\rho_n\rangle_i = \frac{m\langle n\rangle_i}{\int w(r)\,\mathrm{d}v}, \tag{6}$$

where m denotes mass of a particle. Equation (6) shows that the fluid density is approximately proportional to the particle number density. For incompressible flow the fluid density is required to be constant; this is equivalent to the particle number density being constant. The constant value of the particle number density is denoted by n^0.

When multiple materials of different densities are calculated simultaneously, the mass m is changed and the particle number density n^0 is kept constant.

The gradient operator is modelled using the weight function. A gradient vector is evaluated between two neighboring particles i and j as $(\phi_j-\phi_i)(\mathbf{r}_j-\mathbf{r}_i)/|\mathbf{r}_j-\mathbf{r}_i|^2$, where ϕ is a physical quantity. The gradient vector at $\mathbf{r}_i$ is a weighted average of these vectors (Figure 2):

$$\langle\nabla\phi\rangle_i = \frac{d}{n^0}\sum_{j\neq i}\left[\frac{\phi_j-\phi'_i}{|\mathbf{r}_j-\mathbf{r}_i|}(\mathbf{r}_j-\mathbf{r}_i)w(|\mathbf{r}_j-\mathbf{r}_i|)\right], \tag{7}$$

where d is the number of space dimensions. In Equation (7) ϕ'_i is used in place of ϕ_i. If the configuration of neighboring particles is isotropic, Equation (7) is not sensitive to the absolute value. Then, any value can be used for ϕ'_i. Actually, the configuration is not isotropic in general. Thus, the value of ϕ'_i is calculated by

$$\phi'_i = \min(\phi_j) \quad \text{for} \quad \{j \,|\, w(|\mathbf{r}_j-\mathbf{r}_i|)\neq 0\}, \tag{8}$$

in the present study. This means that the minimum value is selected among the neighboring particles within the distance of r_e. Using Equation (8), forces between particles are always repulsive because $\phi_j-\phi'_i$ is positive. According to the authors' experiences, this is good for the numerical stability.

The Laplacian operator is modelled in a transient diffusion problem. Part of a quantity retained by a particle i is distributed to neighboring particles j using the weight function (Figure 3):

$$\Delta\phi_{i\rightarrow j} = \frac{2\,\mathrm{d}\nu\Delta t}{n^0\lambda}\phi_i w(|\mathbf{r}_j-\mathbf{r}_i|), \tag{9}$$

where ν is diffusivity. A parameter λ is introduced so that the variance increase is equal to the analytical solution:

$$\lambda = \int_V w(r) r^2 \, \mathrm{d}v \Big/ \int_V w(r) \mathrm{d}v \tag{10}$$

Diffusion is a linear process, therefore, distributions from one particle to the others can be superposed. Superposition of Equation (9) with respect to j leads to a model of the Laplacian operator:

$$\langle \nabla^2 \phi \rangle_i = \frac{2d}{n^0 \lambda} \sum_{j \neq i} (\phi_j - \phi_i) w(|\mathbf{r}_j - \mathbf{r}_i|). \tag{11}$$

This model is conservative because the quantity lost by a particle i is gained by particles j. Using Equation (11), the Laplacian operator is discretized to simultaneous linear equations with respect to ϕ_i. The central limit theorem guarantees that the iteration of a discretized distribution approaches Gaussian, which is the analytical solution of the transient diffusion problem, providing the variance increase of this distribution is the same as that of the analytical solution.

2.3. Modelling of incompressibility

Incompressibility is represented by keeping the particle number density constant. Here it is assumed that the particle number density n^* deviates from n^0. The particle number density is to be modified to n^0 by n':

$$n^* + n' = n^0. \tag{12}$$

The continuity equation is

$$\frac{1}{\rho}\frac{\mathrm{d}\rho}{\mathrm{d}t} + \nabla \cdot \mathbf{u} = 0. \tag{13}$$

In the MPS method, density is approximated by the particle number density, as shown in Equation (6). Thus, the modification of the particle number density *n'* is related to the modification of the velocity $\mathbf{u}'$ as,

$$\frac{1}{\Delta t}\frac{n'}{n^0} = -\nabla \cdot \mathbf{u}'. \tag{14}$$

The modification of the velocity is derived from the implicit pressure term in the momentum conservation equation in the same way as the simplified MAC (SMAC) method [15]:

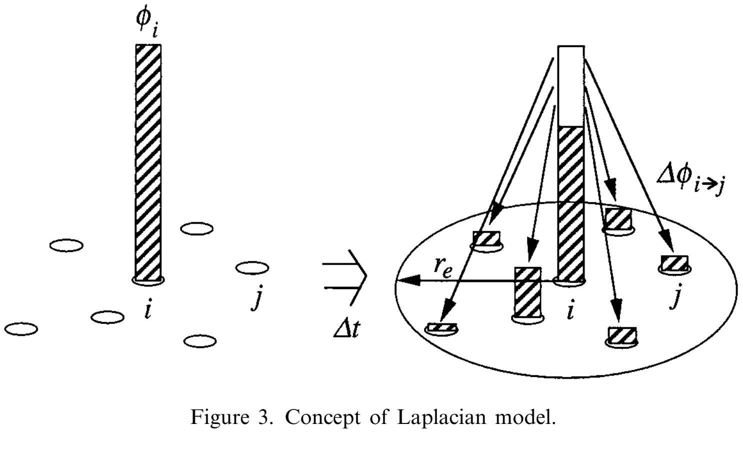

Figure 3. Concept of Laplacian model.

$$\mathbf{u}' = -\frac{\Delta t}{\rho} \nabla P^{n+1}. \tag{15}$$

Substituting Equations (14) and (15) into (12), we have a Poisson equation of pressure:

$$\langle \nabla^2 P^{n+1} \rangle_i = -\frac{\rho}{\Delta t^2} \frac{\langle n^* \rangle_i - n^0}{n^0}. \tag{16}$$

The right side of Equation (16) is the deviation of the particle number density, while it is usually divergence of the velocity vector in the finite difference method. The left side of Equation (16) is discretized to simultaneous linear equations, using the present Laplacian model, Equation (11). The simultaneous linear equations are solved using the incomplete Cholesky decomposition conjugate gradient (ICCG) method [16]. The correction of the velocity vector is calculated by substituting the pressure field into Equation (15). The right side of Equation (15) is discretized using the present gradient model, Equation (7).

In this study, different sizes of the weight function are used. The size which is used for the particle number density and the gradient model is $r_e = 2.1 l_0$, where l_0 is the distance between two adjacent particles in the initial configuration. The value of 2.1 was selected to avoid the concentration of particles near the free surfaces [4]. On the other hand, the size which is used for the Laplacian model is $r_e = 4.0 l_0$. The value of 4.0 was selected by the balance between computation time and accuracy [4].

The weight function used here, Equation (3), is infinity at $r = 0$. With this property the particle number density increases to infinity when the distance between two particles decreases to zero. This leads to a stronger repulsive force between the closer particles through the Poisson equation of pressure. Therefore, clustering of particles is effectively avoided. On the other hand, the particle number density remains a finite value if the weight function is not infinity at $r = 0$. Two particles can occupy the same position with a finite value of the particle number density. This situation is permitted without repulsive forces when $w(0) < n^0$. Thus, clustering is likely to occur.

The flowchart of the calculation algorithm is shown in Figure 4. First, the source terms are explicitly calculated to obtain temporal velocities. Temporal co-ordinates of particles are explicitly calculated by moving particles with the temporal velocities. Next, the Poisson equation of pressure is solved by ICCG with the temporal particle number densities. Finally, new velocities and co-ordinates are obtained from the pressure gradient terms. This algorithm is semi-implicit like the SMAC method [15].

2.4. Boundary conditions

Since no particles exist in the outer region of a free surface, the particle number density decreases at particles on the free surface. Thus, a particle which satisfies

$$\langle n \rangle_i^* < \beta n^0 \tag{17}$$

is considered as on the free surface, where β is a parameter. In this study $\beta = 0.95$. This value was selected by a test calculation [4]. Almost the same solution was obtained between $\beta = 0.8$ and 0.99. A Dirichlet boundary condition of pressure is given to this particle. It is not necessary to outline the free surface in this model. Fragmentation and coalescence of the fluid can be calculated only with this simple rule.

The solid wall boundary condition is simply represented by fixed particles. Three layers of fixed particles are placed in this study. Velocities are always zero at the fixed particles. Pressures are calculated at the particles on the first inner layer to repel the fluid particles from

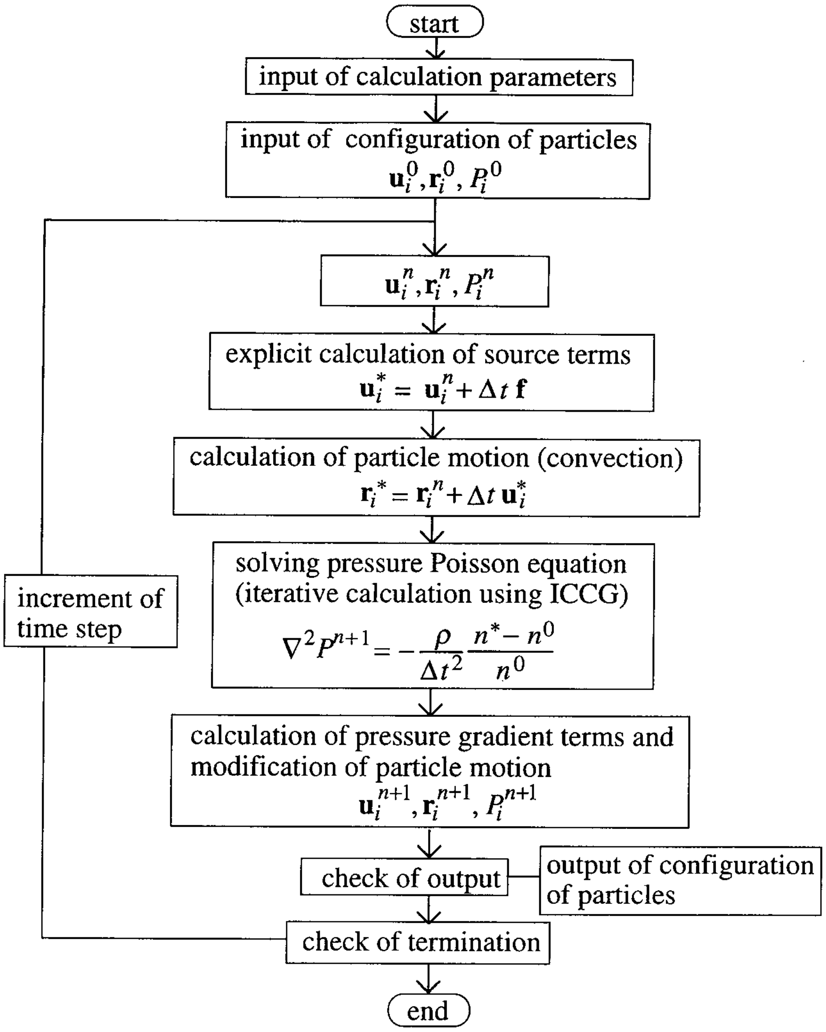
start
input of calculation parameters
input of configuration of particles
$\mathbf{u}_i^0, \mathbf{r}_i^0, P_i^0$
$\mathbf{u}_i^n, \mathbf{r}_i^n, P_i^n$
explicit calculation of source terms
$\mathbf{u}_i^* = \mathbf{u}_i^n + \Delta t\, \mathbf{f}$
calculation of particle motion (convection)
$\mathbf{r}_i^* = \mathbf{r}_i^n + \Delta t\, \mathbf{u}_i^*$
increment of time step
solving pressure Poisson equation (iterative calculation using ICCG)
$\nabla^2 P^{n+1} = -\frac{\rho}{\Delta t^2}\frac{n^* - n^0}{n^0}$
calculation of pressure gradient terms and modification of particle motion
$\mathbf{u}_i^{n+1}, \mathbf{r}_i^{n+1}, P_i^{n+1}$
check of output
output of configuration of particles
check of termination
end

Figure 4. Algorithm of the MPS method.

the wall. Particle number densities are needed for the pressure calculation at theses particles. Since $r_e = 2.1 l_0$, two other layers of fixed dummy particles are located outside of the first layer to keep the particle number density around n^0. Pressures are not calculated at these dummy particles on the outer layer.

2.5. Passively moving solid

A passively moving solid is represented by particles with a fixed relative configuration. When the solid consists of particles i, relationships among co-ordinates of solid particles $\mathbf{r}_i$, the centre of solid $\mathbf{r}_g$, relative co-ordinates of solid particles $\mathbf{q}_i$ and the moment of inertia I are represented by

$$\mathbf{r}_g = \frac{1}{n}\sum_{i=1}^{n} \mathbf{r}_i \tag{18}$$

$$\mathbf{q}_i = \mathbf{r}_i - \mathbf{r}_g, \tag{19}$$

$$I = \sum_{i=1}^{n} |\mathbf{q}_i|^2 \tag{20}$$

In each time step the solid particles are calculated using the same procedure with the fluid particles at first. Next, translation and rotation velocity vectors of the solid are evaluated by

$$\mathbf{T} = \frac{1}{n} \sum_{i=1}^{n} \mathbf{u}_i, \tag{21}$$

$$\mathbf{R} = \frac{1}{I} \sum_{i=1}^{n} \mathbf{u}_i \times \mathbf{q}_i. \tag{22}$$

Finally, the velocity vectors of the solid particles are replaced by those of the solid motion:

$$\mathbf{u}_i = \mathbf{T} + \mathbf{q}_i \times \mathbf{R}. \tag{23}$$

The fluid particles are affected by this motion through the incompressibility calculation in the next time step. This means that the incompressibility condition is temporarily violated.

In this calculation model, the same calculation procedure is applied to both fluid and solid particles at first, and the additional procedure is applied to the solid particles only. If the additional procedure is not applied to the solid particles, they behave as another fluid component.

2.6. Algorithm for list generation

In the MPS method each particle needs a list of neighbors within the distance of r_e. A neighbor of a particle i is identified when the distance from the particle i is less than r_e. The whole list, which should be updated in each time step, requires the scale of N^2 operations for the calculation of distances between all pairs of particles, where N is the number of particles. The list generation is dominant for the computation time in large problems involving many particles.

An algorithm to decrease the count of operations is proposed here. Each particle has two lists; one is for neighbors within the distance of r_e and the other is for candidates of neighbors. A particle is recorded as a candidate when the distance is less than $r_e + h$, where h is an additional distance. Though this calculation also needs the scale of N^2 operations, the list can be updated in each k time steps. The list of neighbors is updated using the list of candidates in each time step. This needs NM_C operations, where M_C is the average number of candidate particles.

Figure 5 shows the CPU time for the list generation with different k. The total number of particles is 2418. The computer is SGI Indy equipped with R4400 (200 MHz). The total CPU time has a minimum point, in this case, at $k_{\text{opt}} = 7$. On the other hand, the CPU time needed for the direct generation of the neighbor list from the distances between all pairs of particles is almost the same as that of $k = 1$ in Figure 5. The proposed algorithm with k_{opt} needs half the CPU time than that of $k = 1$. In general, k_{opt} is proportional to $N^{0.5}M^{-0.5}$. The derivation is specified in the Appendix.

Table 1 shows the principal routines for the CPU time in the MPS code. The CPU time, its fraction to the total and the scale of operation count are provided. The calculation is carried out with the proposed algorithm for the list generation using k_{opt}. The total number of particles is 2418. The most time consuming part of the MPS code is the solver of the Poisson equation of pressure. This part is further divided into three principal steps: matrix generation,

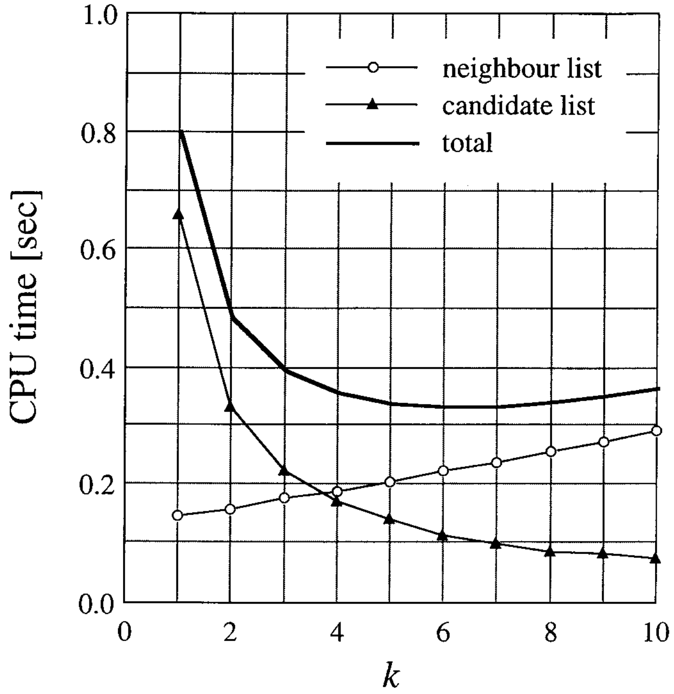

Figure 5. CPU time for neighbor and candidate lists.

incomplete Cholesky decomposition and iteration calculation. The most sensitive routine to the number of particles is the iteration calculation which requires the scale of $N^{1.5}M^{0.5}$ operations. The proposed algorithm for the list generation has the same scale. Therefore, the list generation is no longer dominant for the CPU time in large problems.

3. ANALYSIS OF BREAKING WAVES

3.1. Calculation conditions

The geometry is shown in Figure 6. The calculation is two-dimensional. The fluid is water. Dimensions of the geometry are described in the figure. Viscosity is neglected in this calculation.

Table 1. CPU time of principal routines per time step in the MPS code with 2418 particles

Routine	CPU time [s] (fraction)	Scale of operation count
Matrix generation	0.185 (0.06)	NM
Decomposition	0.974 (0.31)	NM^2
Iteration	1.480 (0.47)	$N^{1.5}M^{0.5}$
List generation	0.188 (0.06)	$N^{1.5}M^{0.5}$
Others	0.334 (0.10)	NM
Total	3.161 (1.00)	

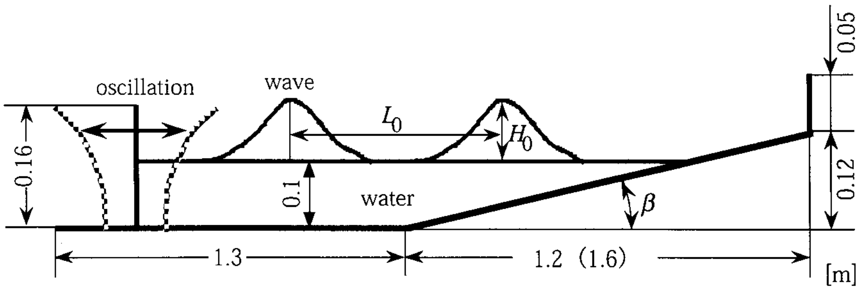

Figure 6. Calculation geometry of breaking waves.

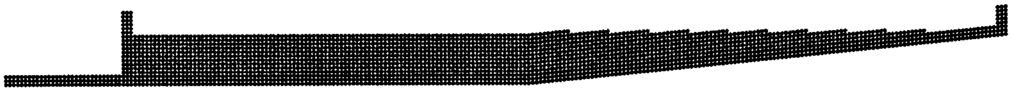

Figure 7. Initial configuration of particles; 2375 particles for $\tan\beta = 0.1$.

The Ursell parameter is defined as,

$$Ur = \frac{HL^2}{h^3}, \tag{24}$$

where H denotes the wave height, L the wave length and h is the depth of water. The following relation can be used for the long wave length:

$$L = T\sqrt{gh}, \tag{25}$$

where T denotes the wave period and g is the acceleration of gravity. In the present calculation, $h = 0.1$ m, $H \cong 0.05$ m and $T = 1.0$–3.2 s. Thus, the Ursell parameter ranges from 50 to 500.

When the Ursell parameter is above 25, cnoidal waves are a good approximation as finite amplitude surface waves [11,12]. A first-order approximation of the cnoidal waves is the $K - dV$ equation, which is not used in this study. A third-order approximation was obtained by Nishikawa *et al.* [17–20]. The shape of the free surface and flow velocity components are calculated from the third-order approximation using a computer code in this study.

The waves are generated by oscillating a vertical wall. The amplitude of the oscillation is vertically changed to follow the velocity profile of the cnoidal wave. It is easy to control the motion of the wall like this in the MPS method, because the wall is also represented by particles. With this fine control of the vertical wall, the cnoidal waves are formed in a short entrance length. This saves the computation time and storage.

Calculations are carried out with two slopes, $\tan\beta = 0.1$ and 0.075. The wave length L_0 is changed from 1.0 to 3.2 m, while the wave height H_0 is little changed around 0.05 m because smaller waves are not suitable for accuracy and larger ones are out of the theory of cnoidal waves. Here, subscript 0 denotes the offshore values. The surf similarity parameter is defined as

$$\xi = \frac{\tan\beta}{\sqrt{H_0/L_0}}, \tag{26}$$

which is used for the classification of breaker types. The total number of particles used is 2375 and 2655 for $\tan\beta = 0.1$ and 0.075, respectively. Dependency on the particle number was not

Table 2. Calculation conditions; $\tan \beta = 0.1$

Period [m]	L_0 [m]	H_0 [m]	ξ
1.0	0.989	0.0564	0.419
1.0	0.989	0.0544	0.426
1.1	1.088	0.0572	0.436
1.2	1.187	0.0630	0.434
1.3	1.286	0.0577	0.472
1.4	1.385	0.0572	0.492
1.5	1.484	0.0585	0.504
1.7	1.681	0.0558	0.549
2.0	1.978	0.0615	0.567
2.0	1.978	0.0548	0.601

investigated in this study. The initial particle configuration is shown in Figure 7. All cases calculated here are summarized in Tables 2 and 3.

The shapes and horizontal velocity profiles of the generated waves are compared with the analytical solutions in the entrance region before the slope. A typical example ($\tan \beta = 0.1$, $L_0 = 1.1$, $H_0 = 0.0572$) is shown in Figure 8. Reflections of the waves are not influential in the calculation because only 3–4 waves are generated. The particles which are regarded as on the free surface are plotted in Figure 8(a). We can see that these particles are enveloped by the analytical solution. The wave shape agrees with the analytical solution. However, the velocity profile shows a difference near the bottom wall as shown in Figure 8(b). This difference is due to the friction with the bottom wall. The friction is derived from the roughness of the wall represented by particles. The fluid particles near the bottom wall go up and down depending on the configuration of the wall particles. This leads to an artificial friction. This friction can occur in the fluid as well. Errors derived from this friction have not been assessed yet.

3.2. Results

Motion of the wave generator and calculation results of typical plunging and spilling breakers are shown in Figures 9 and 10, respectively. These are the second waves generated by the moving wall, because the first waves show different behaviours with the following waves. In Figure 9 the wave is distorted to be asymmetric on the slope and overturning of the wave

Table 3. Calculation conditions; $\tan \beta = 0.075$

Period [m]	L_0 [m]	H_0 [m]	ξ
1.0	0.989	0.0526	0.325
1.3	1.286	0.0536	0.367
1.4	1.385	0.0571	0.369
1.5	1.484	0.0584	0.378
1.6	1.582	0.0573	0.394
1.7	1.681	0.0564	0.409
1.8	1.780	0.0549	0.427
1.9	1.879	0.0534	0.445
2.2	2.176	0.0625	0.443
2.4	2.374	0.0638	0.458
3.2	3.165	0.0564	0.562

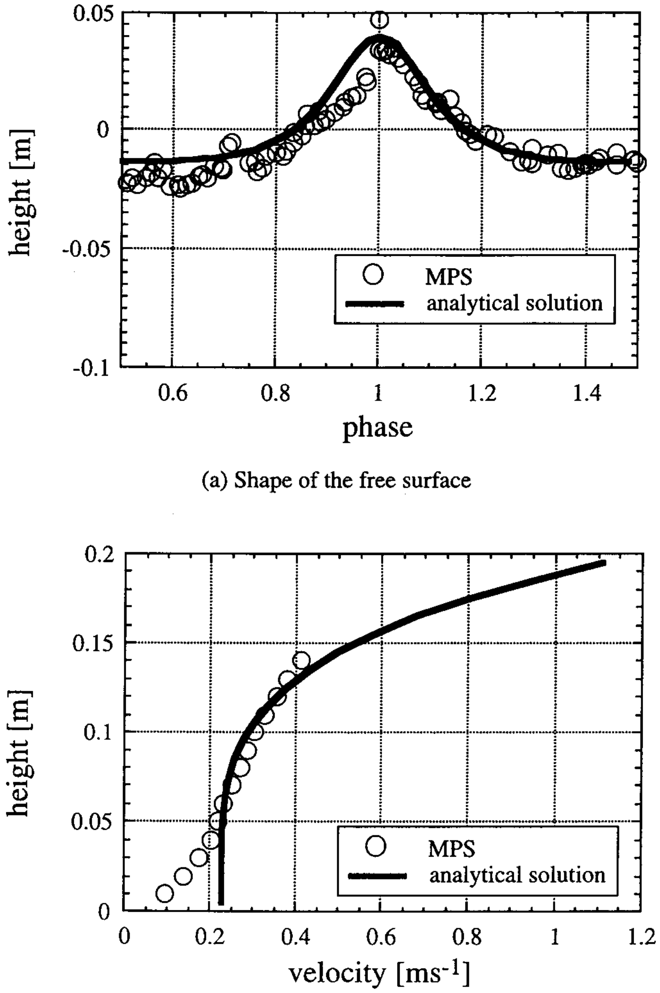

(a) Shape of the free surface

(b) Profile of the horizontal velocity component at the wave centre

Figure 8. Generated non-linear wave ($\tan\beta = 0.1$, $L_0 = 1.1$ m, $H_0 = 0.0572$ m).

front occurs. This is the typical motion of plunging breakers. A line segment drawn from a particle means a velocity vector. We can see large velocities at the top of the wave front. The distortion of the wave is enhanced by the preceding wave which returns offshore on the slope. Thus, the overturning is more likely to occur in the second and following waves. In Figure 10, such distortion is not observed. The wave runs up on the slope by keeping its shape symmetric. The returning flow of the preceding wave is weaker. This is recognized as a spilling breaker.

3.3. Classification of breaker types

To classify the breaker types objectively, an angular momentum of the wave front is introduced. The particles in two regions of the radius r_e are used (Figure 11). One region A_1 is at the top of the wave and the other A_2 is at $L_0/20$ ahead. The angular momentum is defined as

$$\omega = \frac{1}{N} \sum_{i \in A_1, A_2} \mathbf{r}_i \times \mathbf{u}_i \tag{27}$$

where N is the number of particles in A_1 and A_2. Vectors $\mathbf{r}_i$ and $\mathbf{u}_i$ are the positions and the velocities of the particles i, respectively. The origin of the position vectors is the centre between A_1 and A_2. It is expected that this angular momentum is largely negative in plunging breakers. Figure 12(a) shows the change of the angular momentum of the plunging breaker. The angular momentum changes from a small positive value to a large negative value. This change occurs abruptly at the breaking point. On the other hand, it stays around 0.0 in the spilling breaker as shown in Figure 12(b).

Figure 13 shows the minimum values of the angular momentum in all cases calculated in this study. Although the calculation results are scattered, we can see that the minimum angular momentum decreases when the surf similarity parameter, ξ, increases. The larger slope, $\tan\beta = 0.1$, leads to larger angular momentums. These tendencies agree with experiments [13,14]. The value $\omega = -0.006$ is selected as the critical value which classifies the plunging and spilling breakers. When the minimum angular momentum is smaller than the critical value, the breaker type is recognized as plunging. This classification corresponds to the typical behaviour of the plunging breaker: asymmetric shapes and overturning at the wave front.

The breaker types are plotted with the wave steepness, $\sqrt{H_0/L_0}$, and the slope, $\tan\beta$, in Figure 14. Two experimental results are also included in the figure [13,14]. These experiments were carried out using wave tanks. One side of the tank had a piston which generated waves. These waves travelled to the slope on the other side. When $\tan\beta = 0.1$, the critical value is $\xi = 0.45$ in this study. This agrees with Galvin's result [14], but is a little larger than Patrick–Wiegel's result [13] of $\xi = 0.40$. When $\tan\beta = 0.075$, the critical value is not clear in the present study. Both breaker types appear in $\xi = 0.35$–0.45. This transition zone exists between two experimental results. In these experiments, classification of the breaker types was qualitatively carried out by observation. In fact, it was written in Galvin's paper [14] that

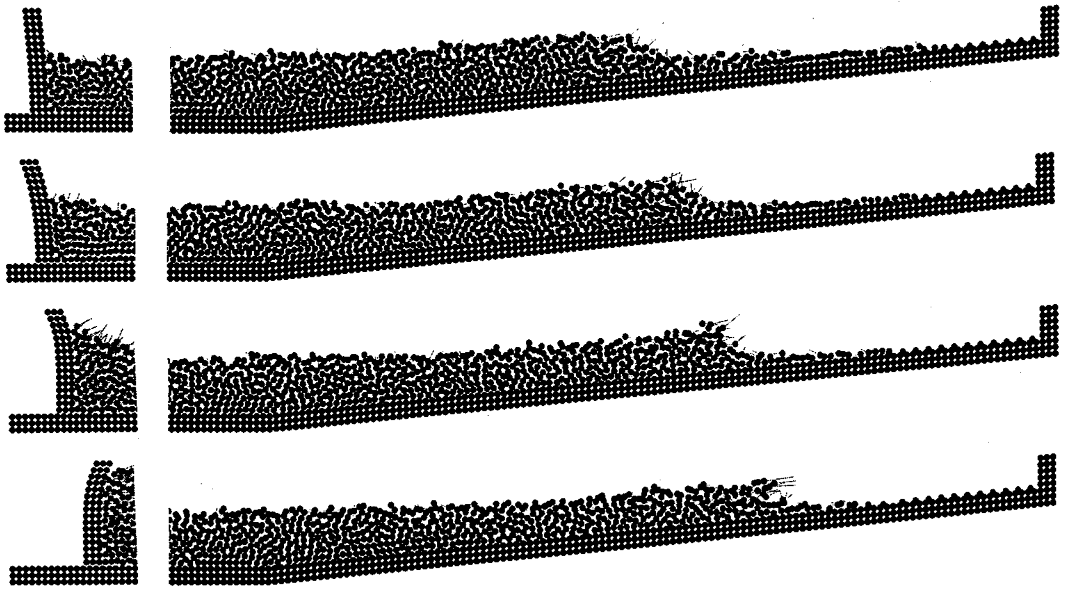

Figure 9. Plunging breaker and motion of the wave generator ($\tan\beta = 0.1$, $L_0 = 1.7$ m, $H_0 = 0.0558$ m, $\xi = 0.549$); time interval = 0.1 s.

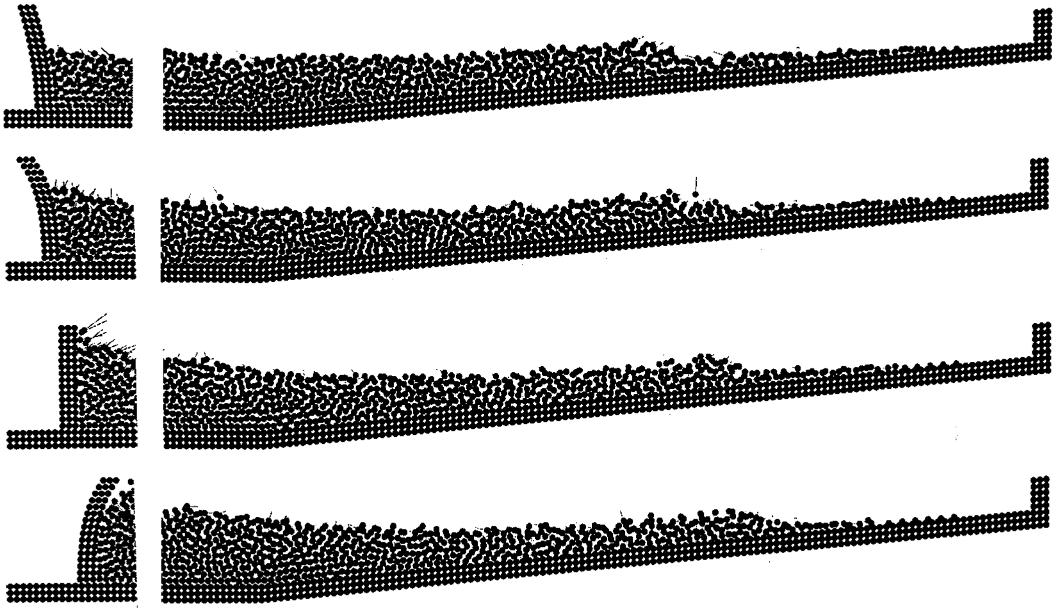

Figure 10. Spilling breaker and motion of the wave generator(tan $\beta = 0.1$, $L_0 = 1.0$ m, $H_0 = 0.0544$ m, $\xi = 0.426$); time interval = 0.1 s.

transitional zones were observed. Consequently, the present calculation results agree with experiments in references.

3.4. Breaking waves with a passively moving float

A floating solid whose density is half of that of water is added to the geometry. The solid consists of 5×5 particles. Initially the float is located above the free surface. When the calculation starts, the float drops into the water due to the gravity. The parameters of

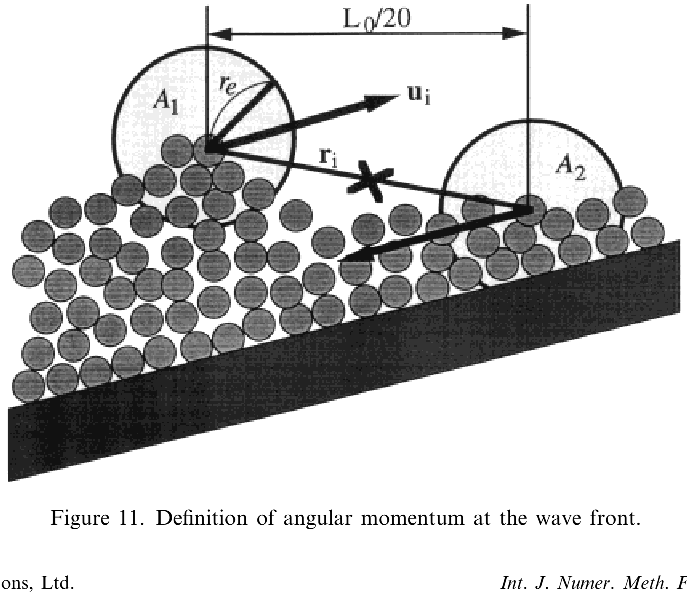

Figure 11. Definition of angular momentum at the wave front.

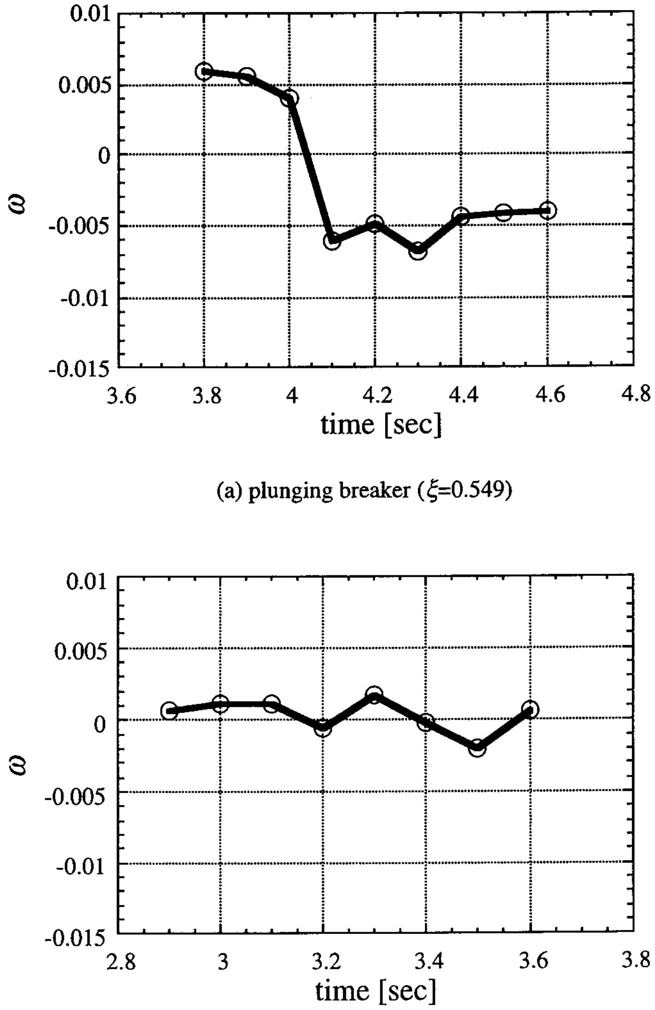

(a) plunging breaker (ξ=0.549)

(b) spilling breaker (ξ=0.426)

Figure 12. Change of angular momentum at the wave front.

generated waves are $\tan \beta = 0.1$, $L_0 = 1.7$ m and $H_0 = 0.0558$ m. This condition is in the region of plunging breakers.

The calculation result is shown in Figure 15 which has five frames with a time interval of 0.2 s. The float is moving offshore with the returning wave in the first frame. The next wave is pushing the float in the second frame. The float is a little rotated by the wave. The float goes up to the wave surface and moves inshore in the third frame. The wave goes faster than the float and the float goes down to the bottom in the following frames. Since friction between the wall and the float is not considered, the float does not stick to the bottom. The float soon begins to move offshore again. This process is repeated when the next wave comes.

The MPS method has possibilities for the analysis of moving interfaces between solids and fluids as well as free surfaces, based on simple calculation models using particles.

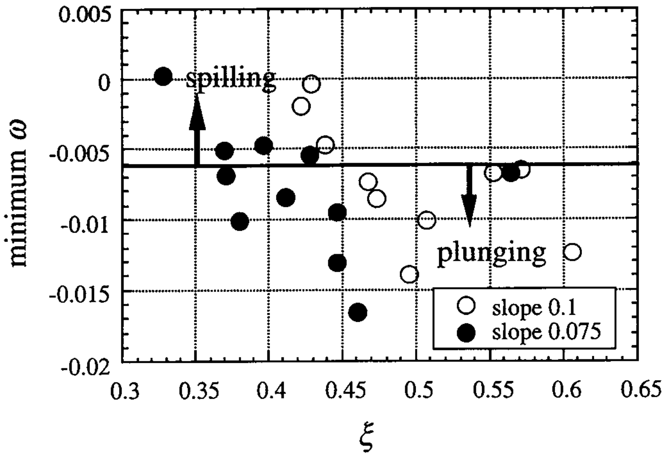

Figure 13. Relation between the minimum angular momentum and surf similarity parameter.

4. CONCLUSIONS

The moving particle semi-implicit (MPS) method is applied to numerical analysis of breaking waves. A calculation model of a passively moving solid is developed to analyze interactions between waves and a float. A list generation algorithm is proposed. Two lists for neighbors and candidates are used in this algorithm. The scale of operation count is reduced from $N^{2.0}$ to $N^{1.5}$.

Numerical calculation of breaking breaks on slopes is carried out using the MPS code. Waves are generated by oscillating a vertical wall, the amplitude of which is vertically changed to follow the cnoidal waves. Shapes of the generated waves agree with the analytical solutions with a short entrance length. The flow velocities near the bottom wall are smaller than the analytical solutions because of the friction with the bottom wall, which is represented by layers of particles.

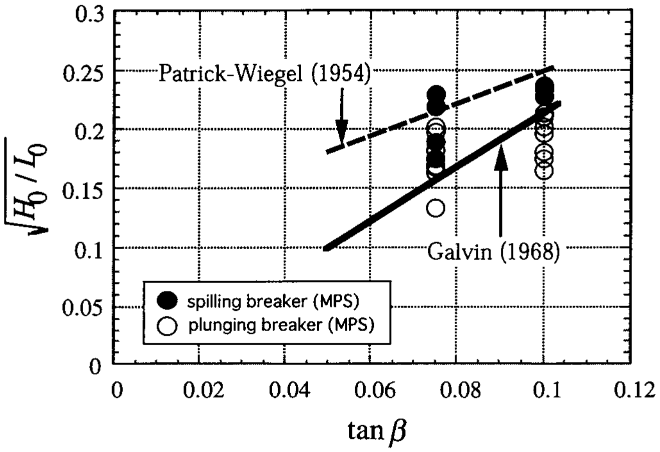

Figure 14. Classification of breaker type.

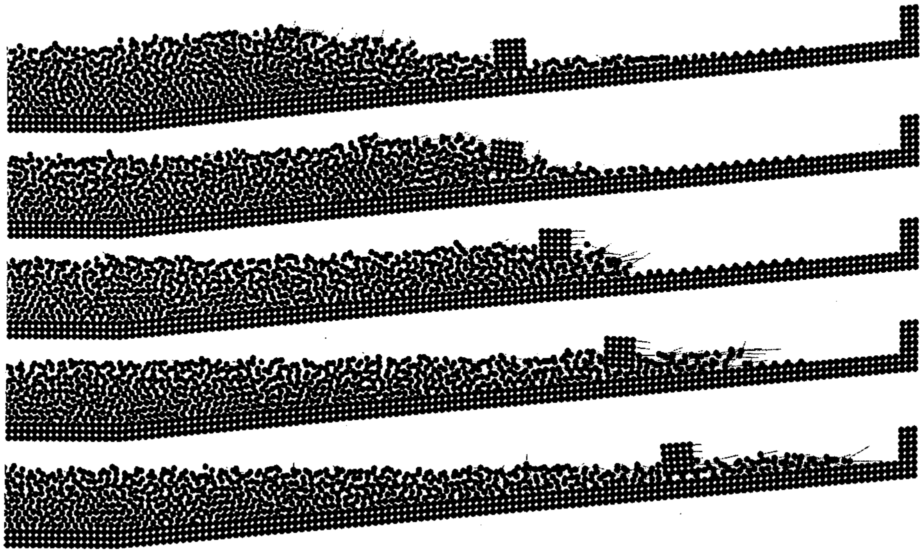

Figure 15. Breaking waves with a floating solid; time interval = 0.2 s.

Spilling and plunging breakers are observed in the calculation results. The angular momentum at the wave front is introduced as a parameter to classify the types of breakers. Plunging breakers occur when the wave steepness is smaller or the slope is steeper. The critical value which separates two breaker types agrees with the experiments in references. The MPS code is also applied to breaking waves with a passively moving float. It is successfully calculated that the float repeatedly moves offshore and inshore.

The MPS method, which is fully based on the Lagrangian description, is applicable to incompressible flows with free surfaces even if fluid fragmentation and coalescence occur. This method has possibilities for fluid–structure interactions when there is a large boundary movement. The MPS method can be easily extended to three dimensions because all particle interaction models are based on the distance between two particles. However, artificial friction, which is derived from the disturbed motion of particles, causes errors which have not been assessed yet.

ACKNOWLEDGMENTS

The authors would like to acknowledge helpful discussions with Dr. T. Sakakiyama and Dr. N. Tanaka of the Central Research Institute of Electric Power Industry.

APPENDIX A. OPTIMIZATION OF THE LIST GENERATION ALGORITHM

Two lists are used in this algorithm; one is for neighbors within the distance of r_e and the other is for candidates of neighbors within the distance of $r_e + h$. The list of neighbors is updated in each time step from the list of candidates. The list of candidates is updated in each k time steps from all particles. Thus, the relation between h and k can be obtained so that all particles entering within the distance of r_e should be recorded in the list of candidates.

Since the motion of particles is explicitly calculated in the MPS method, the time step is restricted by the Courant condition for numerical stability. In this study the Courant limit C is 0.2:

$$C = \frac{\Delta t u_{\max}}{l_0} = 0.2, \tag{A.1}$$

where l_0 is the distance between two adjacent particles in the initial configuration. With the Courant limit, the distance between a pair of particles can decrease by

$$\Delta r = 2Cl_0 \tag{A.2}$$

at most in one time step. Thus, all neighboring particles are still recorded in the list of candidates for k time steps if

$$h = 2kCl_0. \tag{A.3}$$

The number of candidate particles increases with k:

$$M_c = \left(\frac{r_e + 2kCl_0}{r_e}\right)^d M. \tag{A.4}$$

where d is the number of space dimensions and M is the number of neighboring particles. The computation time of the list generation of neighbors is

$$t_n = a\left(\frac{r_e + 2kCl_0}{r_e}\right)^d NM, \tag{A.5}$$

while that of the list generation of candidates per time step is

$$t_c = b\frac{1}{k}N^2. \tag{A.6}$$

Here a and b are constants. The total computation time is

$$t = t_n + t_c \cong a\left(1 + \frac{2dkCl_0}{r_e}\right)NM + b\frac{1}{k}N^2, \tag{A.7}$$

where higher order terms with respect to d are neglected. Equation (A.7) has a minimum point at

$$k_{\text{opt}} = \sqrt{\frac{b\mathrm{r_e N}}{2adCl_0 M}}. \tag{A.8}$$

The CPU times of list generation of neighbors and candidates are approximately proportional to NMk and N^2k^{-1}, respectively, as shown in Equation(A.7). With k_{opt}, which is proportional to $N^{0.5}M^{-0.5}$, the count of operations has the scale of $N^{1.5}M^{0.5}$ for both list generation calculations.

REFERENCES

1. S. Koshizuka, H. Tamako and Y. Oka, 'A particle method for incompressible viscous flow with fluid fragmentation', *Comput. Fluid Dyn. J.* **4**, 29–46 (1995).
2. S. Koshizuka, Y. Oka and H. Tamako, 'A particle method for calculating fragmentation of incompressible viscous fluid', *Proc. Int. Conf: Mathematics and Computations, Reactor Physics and Environmental Analyses*, pp. 1514–1521, 1995.

3. S. Koshizuka and Y. Oka, 'Development of a particle method for calculating fragmentation of incompressible viscous fluid', *Proc. US–Japan Joint Seminar: A Multidisciplinary Int. Seminar Intense Multiphase Interactions*, pp. 145–158, 1995.
4. S. Koshizuka and Y. Oka, 'Moving-particle semi-implicit method for fragmentation of incompressible fluid', *Nucl. Sci. Eng.* **123**, 421–434 (1996).
5. H. Miyata, 'Finite-difference simulation of breaking waves', *J. Comput. Phys.* **65**, 179–214 (1986).
6. K. Takikawa, F. Yamada, M. Arimoto and M. Tabuchi, 'Numerical analysis of internal structure of wave breaking processes on a slope', *Proc. Coast. Eng., JSCE*, **38**, 61–65 (1991) (in Japanese).
7. T. Nakayama and M. Mori, 'An Eulerian finite element method for time dependent free surface problems in hydrodynamics', *Int. j. numer. methods fluids*, **22**, 175–194 (1996).
8. W. Maschek, C.D. Munz and L. Meyer, 'Investigations of sloshing fluid motions in pools related to recriticalities in liquid–metal fast breeder reactor core meltdown accidents', *Nucl. Technol.* **98**, 27–43 (1992).
9. H.A.H. Petit, P. Tonjes, M.R.A. van Gent and O. van den Bosch, 'Numerical simulation and validation of plunging breakers using a 2D Navier–Stokes model', *Proc. 24th Int. Conf. Coastal Eng.*, pp. 511–524, 1994.
10. M.R.A. van Gent, P. Tonjes, H.A.H. Petit and O. van den Bosch, 'Wave action on and in permeable structures', *Proc. 24th Int. Conf: Coastal Eng.*, pp. 1739–1753, 1994.
11. T. Sakakiyama and R. Kajima, 'Numerical simulation of nonlinear wave interacting with permeable breakwaters', *Proc. 23rd Int. Conf. Coastal Eng.*, pp. 1517–1530, 1992.
12. T. Sakakiyama, 'Numerical simulation of nonlinear wave over permeable submerged breakwater', *FED-238*, *Proc. ASME Fluids Eng. Div. Conf: 3*, pp. 391–396, 1996.
13. D.A. Patrick and R.L. Wiegel, 'Amphibian tractors in the surf', *Conf: Ships and Waves* **1**, 397 (1954).
14. C.J. Galvin, Jr., 'Breaker type classification on three laboratory beaches', *J. Geophys. Res.* **73**, 3651–3659 (1968).
15. A.A. Amsden and F.H. Harlow, 'The SMAC method: a numerical technique for calculating incompressible fluid flows', *LA-4370* (1970).
16. C. Hirsch, *Numerical Computation of Internal and External Flows*, Wiley, New York, 1990.
17. H. Nishimura, M. Isobe and K. Horikawa, 'Higher order solutions of the Stokes and the cnoidal waves', *J. Fac. Eng. Univ. Tokyo, Ser. B* **34**, 267–293 (1977).
18. H. Nishimura and M. Isobe, 'On the validities of finite amplitude wave theories', *Proc. Int. Conf: Water Resources Eng.*, pp. 363–374, 1978.
19. M. Isobe, H. Nishimura and K. Horikawa, 'Expressions of perturbation solutions for conservative waves by using wave height', *Proc. 33rd Annul Conf. JSCE*, II, pp. 760–761, 1978 (in Japanese).
20. K. Horikawa, *Nearshore Dynamics and Coastal Processes*, University of Tokyo Press, Tokyo, 1988.